Massless Dirac-Weyl fermions in a $\mathcal{T}_3$ optical lattice

D. Bercioux,[1,2,*] D. F. Urban,[2,3] H. Grabert,[1,2] and W. Häusler[2,4]
[1]*Freiburg Institute for Advanced Studies, Albert-Ludwigs-Universität, D-79104 Freiburg, Germany*
[2]*Physikalisches Institut, Albert-Ludwigs-Universität, D-79104 Freiburg, Germany*
[3]*Departamento de Física de la Materia Condensada C-XII, Facultad de Ciencias, Universidad Autónoma de Madrid, E-28049 Madrid, Spain*
[4]*Institut für Physik, Universität Augsburg, D-86135 Augsburg, Germany*

(Received 28 July 2009; revised manuscript received 7 October 2009; published 1 December 2009)

We propose an experimental setup for the observation of quasirelativistic massless fermions. It is based on a $\mathcal{T}_3$ optical lattice, realized by three pairs of counterpropagating lasers, filled with fermionic cold atoms. We show that in the long wavelength approximation the $\mathcal{T}_3$ Hamiltonian generalizes the Dirac-Weyl Hamiltonian for the honeycomb lattice, however, with a larger value of the pseudospin $S=1$. In addition to the Dirac cones, the spectrum includes a dispersionless branch of localized states producing a finite jump in the atomic density. Furthermore, implications for the Landau levels are discussed.

DOI: 10.1103/PhysRevA.80.063603 PACS number(s): 67.85.−d, 05.30.Fk, 71.10.−w, 71.70.Di

In the past decade, ultracold atoms have emerged as a fascinating new area linking quantum optics with solid state physics [1]. Essentially, these are the only quantum many-body systems for which the particle interaction is both rather precisely known and controllable. In particular, cold atoms confined in optical lattices (OLs) [2] often present systems with crystalline structure in various spatial dimensions $d=1,2,3$ described by textbook models from solid state physics with tunable parameters. This implements Feynman's pioneering idea of quantum simulations using one physical system to investigate another one [3]. A celebrated example [4] is the optical realization of the Mott transition, a well-known phenomenon in solid state physics, describing the transition from a metal to an insulator with increasing interaction strength. Furthermore, the possibility to realize an effective magnetic field by rotation of cold atoms in OLs [5] has opened up prospects of studying other fundamental phenomena in a controlled manner such as the fractional quantum-Hall effect in $d=2$ [6].

The recent preparation of single layers of graphene [7] has attracted considerable attention, since this solid state system displays quasirelativistic motion of electrons on a two-dimensional honeycomb lattice (HCL). However, e.g., due to disorder or impurities, many properties of real graphene cannot fully be accounted for by the idealized Dirac-Weyl Hamiltonian. In this paper we present a detailed study of the $\mathcal{T}_3$ lattice [8] and show that cold fermionic atoms in such an OL indeed behave as quasirelativistic massless Dirac-Weyl fermions. Yet, the $\mathcal{T}_3$ lattice replaces the pseudospin $S=1/2$ of Dirac-Weyl particles in the HCL by the larger value $S=1$. As one of its crucial features, the $\mathcal{T}_3$ lattice exhibits nodes with unequal connectivity. The corresponding class of two-dimensional lattices, specifically *bipartite* lattices, has been studied extensively in the past, with a particular focus on topological localization [9,8], frustration in a magnetic field [10,11], and effects of spin-orbit coupling [12]. The $\mathcal{T}_3$ lattice, illustrated in Fig. 1(a), has a unit cell with three different lattice sites, one sixfold coordinated site H, called *hub*, and two threefold coordinated sites A and B, called *rims*. All nearest-neighbor pairs are formed by a rim and a hub. The energy spectrum [8,10] of the $\mathcal{T}_3$ lattice exhibits particle-hole symmetry and is characterized by three branches. Two of them are linearly dispersing near the K points, in direct analogy to the energy dispersion known from the HCL [7]. The third branch is dispersionless, constantly equal to zero energy. These localized states correspond to nontrivial solutions of the Bloch equations for which the wave functions vanish identically on the hub sites and have opposite amplitudes on the two different rim sites. Localization giving rise to these dispersionless states has a purely topological origin [9] and is quite robust against disorder [8].

In this paper we focus on low energy, long wavelength properties of noninteracting fermions in the $\mathcal{T}_3$ lattice near half filling. As a main result we find that in this parameter range the dynamics is governed by a Hamiltonian of the Dirac-Weyl form

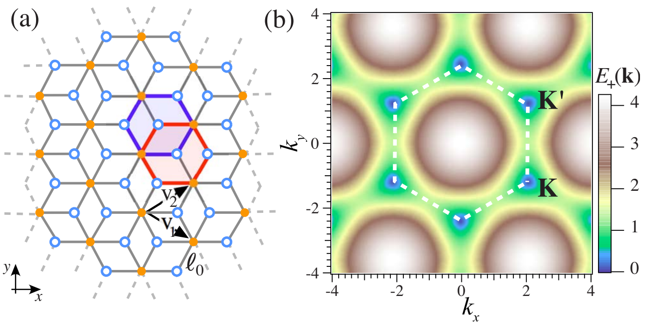

FIG. 1. (Color online) (a) The $\mathcal{T}_3$ lattice. It is characterized by translation vectors $\mathbf{v}_1=(3/2;-\sqrt{3}/2)\ell_0$ and $\mathbf{v}_2=(3/2;\sqrt{3}/2)\ell_0$, with lattice constant ℓ_0. Open circles mark the two sublattices A and B, forming a HCL. Solid circles mark the hub sites H forming a (larger) triangular lattice. (b) Contour plot of $E_+(\mathbf{k})$ in units of the hopping energy t, cf. Eq. (3b). The dashed hexagon defines the first Brillouin zone, $\mathbf{K}=2\pi\ell_0^{-1}(1/3;-\sqrt{3}/9)$ and $\mathbf{K}'=2\pi\ell_0^{-1}(1/3;\sqrt{3}/9)$ are two nonequivalent Dirac points.

---

[*] dario.bercioux@frias.uni-freiburg.de

©2009 The American Physical Society

$$\mathcal{H} = v_{\mathrm{F}} \mathbf{S} \cdot \left(\mathbf{p} - \frac{e}{c} \mathbf{A} \right). \tag{1}$$

Here, v_{F} is the Fermi velocity, $\mathbf{p}=-\mathrm{i}(\partial_x, \partial_y, 0)$ the momentum operator (we set $\hbar=1$) in the lattice xy plane, and $\mathbf{A}$ the vector potential associated with a magnetic field $\mathbf{B}=(\partial_x A_y - \partial_y A_x)\mathbf{e}_z$ perpendicular to the plane. Equation (1) strikingly resembles the Hamiltonian for fermions in graphene. However, as decisive difference, the pseudospin vector $\mathbf{S}=(S_x, S_y, S_z)$ now has total spin $S=1$ reflecting the three inequivalent lattice sites per unit cell in $\mathcal{T}_3$, compared to two in the HCL. In the basis of the eigenstates of S_z the spin operators of Eq. (1) can be expressed as 3×3 matrices

$$S_x = \frac{1}{\sqrt{2}} \begin{pmatrix} 0 & 1 & 0 \\ 1 & 0 & 1 \\ 0 & 1 & 0 \end{pmatrix}, \quad S_y = \frac{1}{\sqrt{2}} \begin{pmatrix} 0 & -\mathrm{i} & 0 \\ \mathrm{i} & 0 & -\mathrm{i} \\ 0 & \mathrm{i} & 0 \end{pmatrix},$$

$$S_z = \begin{pmatrix} 1 & 0 & 0 \\ 0 & 0 & 0 \\ 0 & 0 & -1 \end{pmatrix},$$

which satisfy angular momentum commutation relations.

For zero magnetic field the Hamiltonian (1) is obtained by starting from the Schrödinger equation for the $\mathcal{T}_3$ lattice in the tight-binding approximation,

$$E\Psi_{\mathrm{H}}(\mathbf{R}_{\mathrm{H}}) = -t \sum_j \Psi_{\mathrm{A}}(\mathbf{R}_{\mathrm{H}} + \tau_j) + \Psi_{\mathrm{B}}(\mathbf{R}_{\mathrm{H}} + \tau_{j+1}), \tag{2a}$$

$$E\Psi_{\alpha}(\mathbf{R}_{\alpha}) = -t \sum_j \Psi_{\mathrm{H}}(\mathbf{R}_{\alpha} - \tau_j), \quad \alpha \in \{\mathrm{A}, \mathrm{B}\}. \tag{2b}$$

Here, $\Psi_\alpha(\mathbf{R}_\alpha)$ is the amplitude of the wave function on sublattice $\alpha=\mathrm{A}, \mathrm{H}, \mathrm{B}$, and the τ_j connect nearest neighbors. Solving Eq. (2), we obtain the energy spectrum

$$E_0(\mathbf{k}) = 0, \tag{3a}$$

$$\begin{aligned} E_{\pm}(\mathbf{k}) = \pm t[6 + 4\{\cos[(\mathbf{v}_2 - \mathbf{v}_1) \cdot \mathbf{k}] + \cos[\mathbf{v}_1 \cdot \mathbf{k}] \\ + \cos[\mathbf{v}_2 \cdot \mathbf{k}]\}]^{1/2}, \end{aligned} \tag{3b}$$

where $E_{\pm}$ exhibit a linear dispersion, with Fermi velocity $v_{\mathrm{F}}=3t\ell_0/\sqrt{2}$ [13], about either of the Dirac-points $\mathbf{K}$ and $\mathbf{K}'$, as seen in Fig. 1(b). Next we perform a long wavelength approximation about $\mathbf{K}$

$$\Psi_\alpha(\mathbf{R}_\alpha) = \mathrm{e}^{\mathrm{i}\mathbf{K} \cdot \mathbf{R}_\alpha} \psi_\alpha(\mathbf{R}_\alpha) \tag{4}$$

by separating out the slowly varying part ψ_α of the amplitude. Similarly, we can treat the neighborhood of $\mathbf{K}'$. In the absence of short wavelength scattering processes, wave functions from the vicinities of $\mathbf{K}$ and $\mathbf{K}'$ can be mapped onto each other by interchanging the two rim components so that we focus on the vicinity of $\mathbf{K}$ in the following. Inserting Ψ_α into Eq. (2) finally yields the result (1) when arranging the components $\alpha=\{\mathrm{A}, \mathrm{H}, \mathrm{B}\}$ into a pseudospin triplet and expanding to linear order in $\kappa=|\mathbf{k}-\mathbf{K}|$ for $\kappa \ll |\mathbf{K}|$.

Since $[\mathcal{H}, \mathcal{J}_z]=0$, where $\mathcal{J}_z=L_z+S_z$ is the z component of the total angular momentum and $L_z=-\mathrm{i}\partial_\varphi$, we can choose simultaneous eigenstates of $\mathcal{H}$ and $\mathcal{J}_z$. At nonzero energy $E=\pm v_{\mathrm{F}}\kappa$ these read in polar coordinates (r, φ)

$$\begin{pmatrix} \psi_{\mathrm{A}} \\ \psi_{\mathrm{H}} \\ \psi_{\mathrm{B}} \end{pmatrix} = \mathcal{N} \begin{pmatrix} \xi_- J_{|m|-\xi_-}(\kappa r) \mathrm{e}^{\mathrm{i}(m-1)\varphi} \\ \mathrm{sgn}\,(E) \mathrm{i} \sqrt{2} J_{|m|}(\kappa r) \mathrm{e}^{\mathrm{i}m\varphi} \\ -\xi_+ J_{|m|+\xi_+}(\kappa r) \mathrm{e}^{\mathrm{i}(m+1)\varphi} \end{pmatrix}, \tag{5}$$

with integer m, the eigenvalue of $\mathcal{J}_z$. Here, $J_m(x)$ is a Bessel function, $\xi_{\pm}=\mathrm{sgn}(m \pm 0^+)$, where the infinitesimal 0^+ ensures the correct values for $m=0$, and $\mathcal{N}$ is a normalization constant. The eigenstates at zero energy are given by

$$\begin{pmatrix} \psi_{\mathrm{A}} \\ \psi_{\mathrm{H}} \\ \psi_{\mathrm{B}} \end{pmatrix} = \tilde{\mathcal{N}} \begin{pmatrix} \xi_- J_{|m|-\xi_-}(\kappa r) \mathrm{e}^{\mathrm{i}(m-1)\varphi} \\ 0 \\ \xi_+ J_{|m|+\xi_+}(\kappa r) \mathrm{e}^{\mathrm{i}(m+1)\varphi} \end{pmatrix}, \tag{6}$$

where $\tilde{\mathcal{N}}$ is again a normalization constant. This solution has a finite amplitude only on the rim sites which thus are *topologically* disconnected. The zero-energy solution (6) is infinitely degenerate with respect to the quantum numbers κ and m. The properties of this level, e.g., the deltalike singularity in the density of states, are distinctive features of the $\mathcal{T}_3$ lattice and its Dirac-Weyl behavior, as we shall see below.

Let us now consider the Hamiltonian (1) in a perpendicular, effective magnetic field. We use the symmetric gauge $\mathbf{A}=B(-y, x, 0)/2$. Defining the magnetic length $\ell_B=\sqrt{2c/eB}$, the cyclotron frequency $\omega_{\mathrm{c}}=v_{\mathrm{F}}/\ell_B$, and the dimensionless radial coordinate $\rho=r/\ell_B$, the Schrödinger equation for eigenenergy $E=\omega_{\mathrm{c}}\varepsilon$ reads

$$\omega_{\mathrm{c}} \begin{pmatrix} -\varepsilon & \mathcal{A} & 0 \\ \mathcal{A}^\dagger & -\varepsilon & \mathcal{A} \\ 0 & \mathcal{A}^\dagger & -\varepsilon \end{pmatrix} \begin{pmatrix} \psi_{\mathrm{A}} \\ \psi_{\mathrm{H}} \\ \psi_{\mathrm{B}} \end{pmatrix} = 0. \tag{7}$$

Here $\mathcal{A}=\frac{\mathrm{i}}{\sqrt{2}}\mathrm{e}^{-\mathrm{i}\varphi}(-\partial_\rho+\rho-L_z/\rho)$. The set of first-order differential equations (7) can be recast into second-order differential equations. For the hub component $\psi_{\mathrm{H}}(\rho, \varphi) \propto \phi_{\mathrm{H}}(\rho)\mathrm{e}^{\mathrm{i}m\varphi}$ we get

$$\phi_{\mathrm{H}}''(\rho) + \frac{\phi_{\mathrm{H}}'(\rho)}{\rho} + \left(2m - \rho^2 - \frac{m^2}{\rho^2} + \varepsilon^2 \right) \phi_{\mathrm{H}}(\rho) = 0 \tag{8}$$

and similar equations hold for $\phi_{\mathrm{A/B}}(\rho)$. The general solution at $\varepsilon \neq 0$ is given by

$$\begin{pmatrix} \psi_{\mathrm{A}} \\ \psi_{\mathrm{H}} \\ \psi_{\mathrm{B}} \end{pmatrix} = \begin{pmatrix} \mathcal{N}_{\mathrm{A}} \rho^{|m|-\xi_-} L_{n+\eta_-}^{|m|-\xi_-}(\rho^2) \mathrm{e}^{\mathrm{i}(m-1)\varphi} \\ \mathcal{N}_{\mathrm{H}}\, \mathrm{sgn}\,(E) \rho^{|m|} L_n^{|m|}(\rho^2) \mathrm{e}^{\mathrm{i}m\varphi} \\ \mathcal{N}_{\mathrm{B}} \rho^{|m|+\xi_+} L_{n-\eta_+}^{|m|+\xi_+}(\rho^2) \mathrm{e}^{\mathrm{i}(m+1)\varphi} \end{pmatrix} \mathrm{e}^{-\rho^2/2} \tag{9}$$

with integer m and positive integer n. The $\mathcal{N}_\alpha$ are appropriate numerical factors [14]. Here, $L_a^b(x)$ is an associated Laguerre polynomial of order $a \geq 0$, and $\eta_{\pm}=\theta(m \pm 0^+)$, where θ is the unit-step function. The eigenenergies of the states (9), the *Landau levels*, are found to read

$$E_{n,m} = \pm 2\omega_{\mathrm{c}} \sqrt{n + |m|\theta(-m) + \frac{1}{2}}. \tag{10}$$

They scale with the square root of the index n and m and display a finite energy value even for $n=m=0$. These peculiarities are in analogy with the unusual Landau levels of the HCL that have received broad attention in the context of graphene [15,16].

Equation (7) deserves special care at zero energy. Then, two solutions are allowed: a zero-energy Landau level and a topological solution. The former is characterized by a single nonvanishing component,

$$\psi_{\mathrm{A}} \propto \mathrm{e}^{-\rho^2/2}\rho^{m-1}\mathrm{e}^{\mathrm{i}(m-1)\varphi} \tag{11}$$

with $m \geq 1$ [17]. The other solution has a vanishing hub component and reads

$$\begin{pmatrix}\psi_{\mathrm{A}}\\ \psi_{\mathrm{H}}\\ \psi_{\mathrm{B}}\end{pmatrix} = \begin{pmatrix}\tilde{\mathcal{N}}_{\mathrm{A}}\rho^{|m|-\xi_-}L_{n+\eta_-}^{|m|-\xi_-}(\rho^2)\mathrm{e}^{\mathrm{i}(m-1)\varphi}\\ 0\\ \tilde{\mathcal{N}}_{\mathrm{B}}\rho^{|m|+\xi_+}L_{n-\eta_+}^{|m|+\xi_+}(\rho^2)\mathrm{e}^{\mathrm{i}(m+1)\varphi}\end{pmatrix}\mathrm{e}^{-\rho^2/2} \tag{12}$$

with $n \geq 1$ [18]. The zero-energy Landau level (11) has the same degeneracy as the other Landau levels at finite energies (10). In the case of the HCL a similar solution is responsible for the atypical quantum-Hall effect observed in transport experiments through graphene layers [19]. The Atiyah-Singer index theorem [20] connects these zero-energy Landau levels with the structure of the Dirac-Weyl Hamiltonian. Thus, contrary to the finite energy Landau levels, they are robust against fluctuations of the electrostatic and magnetic fields. On the other hand, the existence of the topological solution (12) is due to the bipartite structure of the $\mathcal{T}_3$ lattice. The two types of zero-energy solutions cannot be distinguished on the mesoscopic scale. Their level degeneracies just add up and enhance the total degeneracy at zero energy. This feature should be observable in quantum-Hall effect experiments.

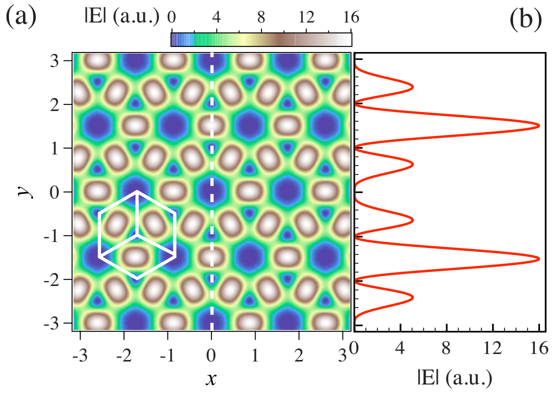

FIG. 2. (Color online) (a) Distribution of the laser field intensity for generating a $\mathcal{T}_3$ lattice. (b) Cut of the field intensity along the y axis.

Experimentally, the $\mathcal{T}_3$ structure can be realized as an OL created by three counterpropagating pairs of laser beams with the same wavelength $\lambda = 3/2\ell_0$ which divide the plane into six sectors of 60°. All six laser beams are linearly polarized with the electrical field in the xy plane. Orienting the polarization of one pair of lasers along the y axis, $\mathbf{E}_1 = (0, E_y, 0)$, the other two pairs are obtained by rotating $\mathbf{E}$ by 120° around the z axis. This arrangement produces the profile of laser intensity depicted in Fig. 2(a); Fig. 2(b) shows a cut of the field intensity along the y axis. It is apparent that the hopping probability between rim sites is exponentially small compared to the hopping probability between neighboring hub-rim pairs. Contrary to other theoretical proposals for the observation of massless fermions in OLs, we do not require the presence of time-dependent potentials [21], staggered gauge fields [22], external gauge fields [23], and the proposed laser configuration does not create spurious lattice minima [24]. The tight-binding Hamiltonian and its long wavelength approximation (1) are valid for a $\mathcal{T}_3$ lattice populated by single-component fermionic atoms, e.g., ^{40}K or ^{6}Li. Indeed, for single-component fermions, the atomic collisions are negligible at low temperature [1]. From the experimental point of view, time-of-flight imaging via light absorption [25] can be used in order to detect the presence of massless Dirac-Weyl fermions. The harmonic trap potential $V(\mathbf{r}) = m\omega^2\mathbf{r}^2/2$ confining the fermionic cold atom gas is ramped down slowly enough for the atoms to stay adiabatically in the lowest band while their quasimomentum is approximately conserved. Under these conditions, free fermions expand with ballistic motion and, from the measured absorption images, it is possible [26,27] to reconstruct the initial reciprocal-space density profile of the trapped gas. Then, the local density approximation is typically well satisfied and the local chemical potential can be assumed to vary with the radial coordinate as $\mu(\mathbf{r}) = \mu_0 - V(\mathbf{r})$, where μ_0 is the chemical potential at the center of the trap. For a system of cold atoms at temperature T, the atomic density is uniquely determined by the chemical potential

$$n(\mu) = \frac{1}{\mathcal{S}_0}\int f(\mathbf{k},\mu)d\mathbf{k}. \tag{13}$$

Here $\mathcal{S}_0$ is the area of the first Brillouin zone of the $\mathcal{T}_3$ lattice, and $f(\mathbf{k},\mu) = \{\exp[(E_\alpha(\mathbf{k}) - \mu)/k_{\mathrm{B}}T] + 1\}^{-1}$ is the Fermi distribution function, where $E_\alpha(\mathbf{k})$ is the energy spectrum of the $\mathcal{T}_3$ lattice, cf. Eq. (3). Figure 3 shows the atomic density n as a function of the chemical potential μ. The contribution from the highly degenerate topological band (6) manifests itself at $\mu = 0$ as a sharp jump in the atomic density. This feature is specific to the $\mathcal{T}_3$ lattice. For small finite μ we see that n increases (decreases) proportional to μ^2, which reflects the

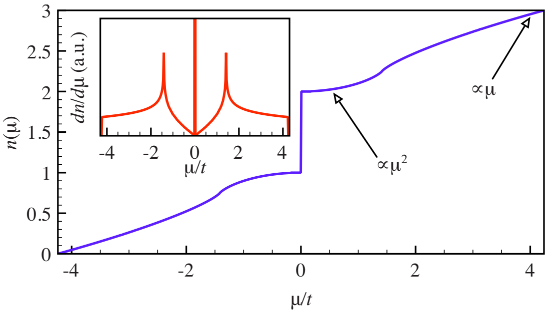

FIG. 3. (Color online) The number of atoms n per unit cell at zero temperature as a function of μ/t, ignoring physical spin and valley degeneracies, where t is the nearest-neighbor hopping amplitude, cf. Eq. (2). Inset: density of states, $dn/d\mu$, versus μ/t.

linear dispersion of massless fermions near the band center as well as particle-hole symmetry [28]. On the contrary, for values of μ close to the maximum or minimum of the energy band, i.e., far away from the band center, where the long wavelength approximation can no longer be applied, n varies proportional to μ.

In conclusion, we have discussed an experimental setup for the observation of Dirac-Weyl fermions in a $\mathcal{T}_3$ OL. In particular, we have shown that in the low energy and long wavelength approximation the $\mathcal{T}_3$ Hamiltonian describes massless Dirac-Weyl fermions. This generalizes results known for the case of the HCL, however, with pseudospin $S=1$. The Dirac cones manifest themselves in a quadratic dependence of the atomic density on the chemical potential. Besides the Dirac-Weyl fermions, the $\mathcal{T}_3$ energy spectrum features a dispersionless branch of localized states. These states give rise to a pronounced finite jump in the atomic density, a hallmark of the $\mathcal{T}_3$ lattice. We have also studied the effects of an effective magnetic field perpendicular to the lattice. This leads to the formation of unusual Landau levels resembling those known for the case of the HCL. In particular a zero-energy Landau level coexists with the dispersionless level of localized states.

We gratefully acknowledge helpful discussions with A. De Martino, R. Egger, T. Esslinger, P. Hänggi, and M. Rizzi. This work was supported by the Excellence Initiative of the German Federal and State Governments.

---

[1] I. Bloch, J. Dalibard, and W. Zwerger, Rev. Mod. Phys. **80**, 885 (2008).
[2] M. Greiner and S. Folling, Nature (London) **453**, 736 (2008).
[3] R. Feynman, Int. J. Theor. Phys. **21**, 467 (1982).
[4] M. Greiner *et al.*, Nature (London) **415**, 39 (2002).
[5] D. Jaksch and P. Zoller, New J. Phys. **5**, 56 (2003); M. Polini, R. Fazio, A. H. MacDonald, and M. P. Tosi, Phys. Rev. Lett. **95**, 010401 (2005); A. Jacob *et al.*, New J. Phys. **10**, 045022 (2008).
[6] A. S. Sørensen, E. Demler, and M. D. Lukin, Phys. Rev. Lett. **94**, 086803 (2005).
[7] A. H. Castro Neto *et al.*, Rev. Mod. Phys. **81**, 109 (2009).
[8] B. Sutherland, Phys. Rev. B **34**, 5208 (1986).
[9] T. Morita and T. Horiguchi, J. Math. Phys. **13**, 1243 (1972).
[10] J. Vidal, R. Mosseri, and B. Douçot, Phys. Rev. Lett. **81**, 5888 (1998).
[11] S. E. Korshunov, Phys. Rev. B **63**, 134503 (2001); M. Rizzi, V. Cataudella, and R. Fazio, *ibid.* **73**, 144511 (2006).
[12] D. Bercioux, M. Governale, V. Cataudella, and V. M. Ramaglia, Phys. Rev. Lett. **93**, 056802 (2004); Phys. Rev. B **72**, 075305 (2005).
[13] Note that v_F differs by a factor $\sqrt{2}$ from the Fermi velocity of a HCL with the same parameters t and ℓ_0.
[14] Numerical factors are $\mathcal{N}_A = n\eta_- + \xi_-$, $\mathcal{N}_H = i\sqrt{2n+1+2|m|\theta(-m)}$, and $\mathcal{N}_B = (1-\delta_{n,0})[(1-\eta_+)(n-m)-\eta_+]$.
[15] G. W. Semenoff, Phys. Rev. Lett. **53**, 2449 (1984).
[16] A. De Martino, L. Dell'Anna, and R. Egger, Phys. Rev. Lett. **98**, 066802 (2007).
[17] For $m<1$ the solution of the associated differential equation is not regular for $\rho \to 0$.
[18] Numerical factors are $\tilde{\mathcal{N}}_A = \eta_+(\xi_- n - 1) + 1$ and $\tilde{\mathcal{N}}_B = (1-\eta_-)(n-m)+1$.
[19] K. S. Novoselov *et al.*, Nature (London) **438**, 197 (2005); Y. Zhang, Y.-W. Tan, H. L. Stormer, and P. Kim, *ibid.* **438**, 201 (2005).
[20] Y. Aharonov and A. Casher, Phys. Rev. A **19**, 2461 (1979); L. Erdös and V. Vougalter, Commun. Math. Phys. **225**, 399 (2002).
[21] L.-K. Lim, C. M. Smith, and A. Hemmerich, Phys. Rev. Lett. **100**, 130402 (2008).
[22] J.-M. Hou, W.-X. Yang, and X.-J. Liu, Phys. Rev. A **79**, 043621 (2009).
[23] N. Goldman, A. Kubasiak, A. Bermudez, P. Gaspard, M. Lewenstein, and M. A. Martin-Delgado, Phys. Rev. Lett. **103**, 035301 (2009).
[24] S.-L. Zhu, B. Wang, and L.-M. Duan, Phys. Rev. Lett. **98**, 260402 (2007).
[25] M. Köhl, H. Moritz, T. Stoferle, K. Gunter, and T. Esslinger, Phys. Rev. Lett. **94**, 080403 (2005).
[26] T. L. Ho and C. V. Ciobanu, Phys. Rev. Lett. **85**, 4648 (2000).
[27] R. O. Umucalılar, H. Zhai, and M. Ö. Oktel, Phys. Rev. Lett. **100**, 070402 (2008).
[28] Actually, a small difference in the on-site energies, ε_H and ε_R for hub and rim sites, respectively, will cause a gap in the dispersing part of the energy spectrum, though leaving the topological band untouched. This then modifies $n(\mu)$ in very close vicinity $\sim|\varepsilon_H - \varepsilon_R|$ of the sharp jump.